universität wien

MASTERARBEIT / MASTER'S THESIS

Titel der Masterarbeit / Title of the Master's Thesis

„Black spinel – a gem material from Bo Phloi, Thailand"

verfasst von / submitted by

Ágnes Blanka Kruzslicz

angestrebter akademischer Grad / in partial fulfilment of the requirements for the degree of

Master of Science (MSc)

Wien, 2019 / Vienna, 2019

Studienkennzahl lt. Studienblatt / degree programme code as it appears on the student record sheet:	A 066 815
Studienrichtung lt. Studienblatt / degree programme as it appears on the student record sheet:	Masterstudium Erdwissenschaften UG2002
Betreut von / Supervisor:	Univ.-Prof. Dr. Lutz Nasdala

Acknowledgement

I am indebted to Prof. Dr Lutz Nasdala and Prof. Dr Manfred Wildner, Dr Radek Škoda, Prof. Dr Günther Redhammer, Prof. Dr Christian Lengauer and Dr Bhuwadol Wanthanachaisaeng for their professional help. I thank Andreas Wagner for sample preparation. Prof. Dr Eugen Libowitzky and Prof. Dr Gerald Giester kindly provided reference samples. I am thankful for the kind help of Ing. Wolfgang Zirbs in technical issues and for the fruitful discussions with Dipl.-Geol. Manuela Zeug and Dr Christoph Lenz. Special thanks to my friends for the fruitful discussions and keeping my vibe alive.

I would like to express my deepest gratitude and dedicate this work to my unborn baby. Without our sacrifice this achievement could have never been put through. Our suffering was not pointless. Thank you from the bottom of my heart!

Table of contents

ABSTRACT (GERMAN)

Das Edelsteinabbaugebiet Bo Phloi befindet sich in der Provinz Kanchanaburi im Westen Thailands, etwa 30 km nördlich der Stadt Kanchanaburi. Die Gegend war berühmt für ihre blauen Saphirkristalle in Edelsteinqualität. Da die Produktion von Korund inzwischen praktisch zum Erliegen gekommen ist, verwenden lokale Edelsteinschleifer, um ihren Lebensunterhalt zu verdienen, den immer noch reichlich vorkommenden schwarzen Spinell und stellen aus diesem verschiedene Arten von Schmuck her. Die vorliegende Arbeit fasst die Ergebnisse einer detaillierten mineralogischen Charakterisierung des Bo Phloi-Materials zusammen. Bei allen Proben handelt es sich um Mg-Al-Spinell ($MgAl_2O_4$) mit erhöhtem Fe-Gehalt (FeO 20.7 ± 0.9 wt%). Basierend auf Mössbauer-spektroskopischen Ergebnissen liegt das Eisen sowohl zwei- als auch dreiwertig vor, wobei letzteres beide Kationenpositionen im Kristallgitter (4er- und 6er-koordiniert) besetzt. Das Fe^{3+} bewirkt daher eine sogenannte „teilweise inverse“ Besetzung der Kationenplätze. Infolgedessen stimmt das Ramanspektrum des Bo Phloi-Spinells nicht mit dem eines „normalen“ Spinells überein, sondern ähnelt viel mehr den Spektren anderer „inverser“ Minerale der Spinellgruppe, wie Hercynit oder Magnesioferrit. Zudem bestimmt der hohe Fe-Gehalt die intensive Einfärbung des Materials. Makroskopische Proben sind scheinbar völlig schwarz, während die graubraune Eigenfarbe des Bo Phloi-Spinells nur bei Probendicken von deutlich unter 0,1 mm beobachtbar ist.

ABSTRACT (ENGLISH)

The Bo Phloi gem field is located in the Kanchanaburi province, western Thailand, about 30 km north of the town of Kanchanaburi. The area was renowned mostly for its gem-quality blue sapphire crystals. As corundum production has now virtually ceased, local gem cutters, in an attempt to make a living, use the still abundantly occurring black spinel to produce various sorts of jewellery. The present thesis summarises the results of a detailed mineralogical characterisation of the Bo Phloi material. All samples were found to be spinel *sensus stricto* ($MgAl_2O_4$) with elevated Fe content (FeO 20.7 ± 0.9 wt%). Based on Mössbauer spectroscopic results, Fe occurs in both di- and trivalent states, the latter occupying both (4- and 6-coordinated) cation sites in the crystal lattice. The Fe^{3+} causes a so-called "partially inverse" occupation of the cation sites. As a result, the Raman spectrum of the Bo Phloi spinel is not at all reminiscent to that of "normal" spinel, but rather similar to other "inverse" spinel-group minerals such as hercynite or magnesioferrite. Also, the high Fe content controls the intense colouration of the material. Macroscopic samples appear black and the greyish brown colour is only observed at sample thicknesses of well below 0.1 mm.

1. INTRODUCTION

1.a Background

The mineral spinel (more precisely magnesium aluminate spinel, $MgAl_2O_4$; cubic space group $Fd\bar{3}m$; Sickafus et al., 1999; compare also Grimes et al., 1983) occurs commonly as idiomorphic to hypidiomorphic grains in basic igneous rocks, in regional and contact metamorphic rocks, and as water-worn pebbles in alluvial sediments. Also, spinel crystals are significant extra-terrestrial materials appearing in lunar rocks and in meteorites (Xirouchakis et al., 2002; Yu and Gee, 2005).

The spinel structure is characterised by O^{2-} ions that form a cubic close-packing (CCP), connected by two non-equivalent cation sites, one 4- and one 6-coordinated with O. Two different site occupations exist. In “normal” spinels – such as $MgAl_2O_4$ – divalent cations occupy the tetrahedral cation site (4-coordination) whereas trivalent cations occupy the octahedral site (6-coordination), resulting in the general formula $A^{2+[4]}\,B^{3+[6]}{}_2\,O_4$. “Inverse” spinels, in contrast, half of the trivalent cations occupy the 4-coordinated site whereas the remaining trivalent cations and divalent cations are incorporated at the 6-coordinated site, resulting in the general formula $B^{3+[4]}\,[A^{2+}B^{3+}]^{[6]}\,O_4$. In nature, however, many spinels represent intermediate states that are characterised by a “partially inverse” site occupation. In such cases, the general formula can be summarised as $(A_{1-i}B_i)^{[4]}\,(A_iB_{2-i})^{[6]}\,O_4$, where i is the inversion parameter. The degree of inversion depends on several factors discussed by O'Neill and Navrotsky (1983); however, it is mainly controlled by the fraction of trivalent cations at the tetrahedral sites.

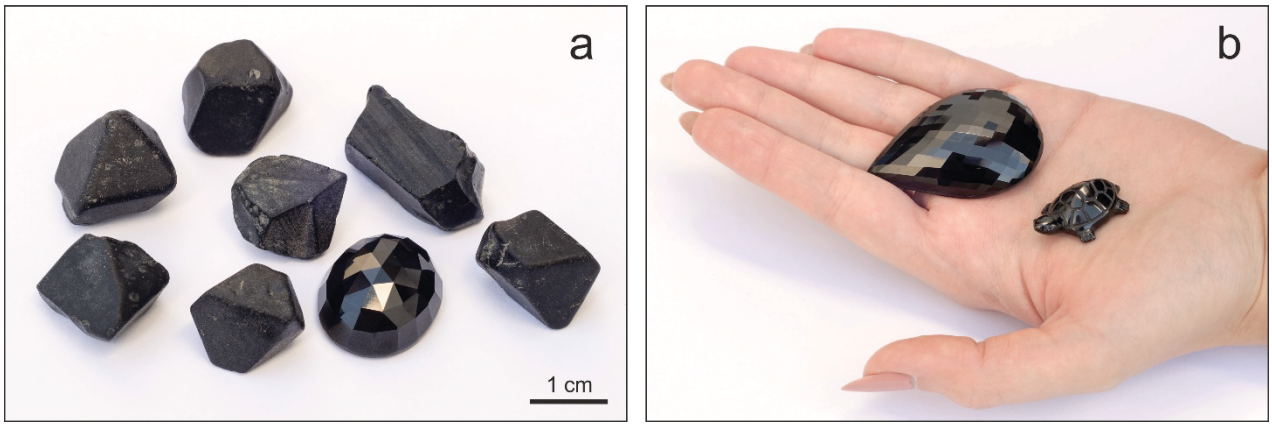

Figure 1: Photographs of rough and polished black spinel specimens from Bo Phloi, Thailand. **(a)** Faceted stone (32.7 ct) and seven rough crystals (24.0–33.7 ct). **(b)** Droplet-shaped, faceted specimen (49.0 mm × 32.4 mm; 167.4 ct) and a small, carved turtle (30.3 ct). Photos by M. Wildner.

Several terms are used in Thailand, and other gem-producing countries, to describe black non-transparent spinel (Figure 1), among which “pleonast” is the most well-known. Local Thai names include “nin” (meaning black gem), “nin-ta-go” or “nin-tan” (both meaning solid looking). Also, many dealers use the misleading term “onyx”

to describe black spinel (Hurwit, 1988). Spinel varieties with elevated iron content are also called “ceylonite” (Deer et al., 1996). With the continuous decline of sapphire production in the Kanchanaburi area, local miners and cutters were obliged to deal with black spinel, in order to cope with the missing income. For this reason, faceted and carved black spinel gems have become more and more widespread in local gem markets.

1.b Geological setting

Cenozoic basaltic bodies in Thailand started to form approximately 10 Ma ago (Figure 2). Volcanism was caused by regional lifting and depressional melting that resulted in extensive basaltic eruptions. The basaltic body of Bo Phloi was supposedly formed either in the Inthanon zone developed within the East Malaya block (Stauffer, 1983) or within the Shan-Thai craton (Barr and Macdonald, 1987). Similar Cenozoic basaltic bodies enclosing large black spinel xenocrysts were discovered in Cambodia, Australia, Tanzania, Vietnam, Myanmar, Sri Lanka, and other parts of Thailand.

The Bo Phloi basaltic body is located in a major fracture zone succeeding on Silurian-Devonian quartzite of the Bo Phloi Formation. On the surface it appears as a remnant small plug approximately 1 km^2 in size (Bunopas and Bunjitradulya, 1975). According to the currently accepted classification, the basalt from Bo Phloi has a nepheline-hawaiite composition (Barr and Macdonald, 1978, 1981; Yaemniyom, 1982). Magma ascended rapidly from the upper mantle (depth of 36 to 79 km) without any significant crustal interaction. Prevailing pressure was approximately 18–25 kbar and the formation temperature ranged between 1340-1475°C (Barr and Macdonald 1981; Ngarmpis, 1982). The basaltic body was dated back to the Pliocene (3.14 ± 0.17 Ma according to Barr and Macdonald, 1981; 4.17 ± 0.11 Ma according to Sutthirat et al., 1994; see also Choowong, 2002).

The Bo Phloi basaltic rock is a dark, dense, extremely fine-grained material with a porphyritic texture. There are abundant mantle xenoliths and xenocrystals such as pyroxene, spinel (Figure 3a), sanidine, olivine, plagioclase, and magnetite. Less common syngenetic constituents include zircon, rutile, sapphire, and ruby.

1.c Mining

Local artisanal mining of gemstones is common in South-East Asia. Besides, some large-scale industrial mines are still in operation in Thailand (Chantaburi, Kanchanaburi, Denchai, Phrae, and Bo Phloi), although the gem mining industry in general has declined appreciably in comparison its zenith in the 1960’s.

The Bo Phloi gem field is located in Western Thailand, about 30 km north of the town of Kanchanaburi (Figure 2). The area (Fig 3b) was renowned for its gem quality blue sapphire (Bunopas and Bunjitadulya, 1975; Vichit et al., 1978). Gemstones are found in residual weathered basaltic soil or gravel deposits that are up to 3 m thick and lie 13–15 m below the surface (Hansawek and Pattamalai, 1997;

Khamloet et al., 2014). The gem-bearing fluvial deposition was dated back to the Pleistocene (approximately 0.7 Ma; Udomchoke, 1988).

Mining in Bo Phloi first started in 1918, but shortly thereafter the deposit was believed to be depleted. In 1987 the site was rediscovered, and large-scale mining commenced lasting only a few years. Currently the production has almost ended and areas are being transformed, at least supposedly, for recreational purposes (note that the currently still most promising gem area is located within what is now called a "golf course"). Since the decrease of blue sapphire production, focus has shifted towards black spinel.

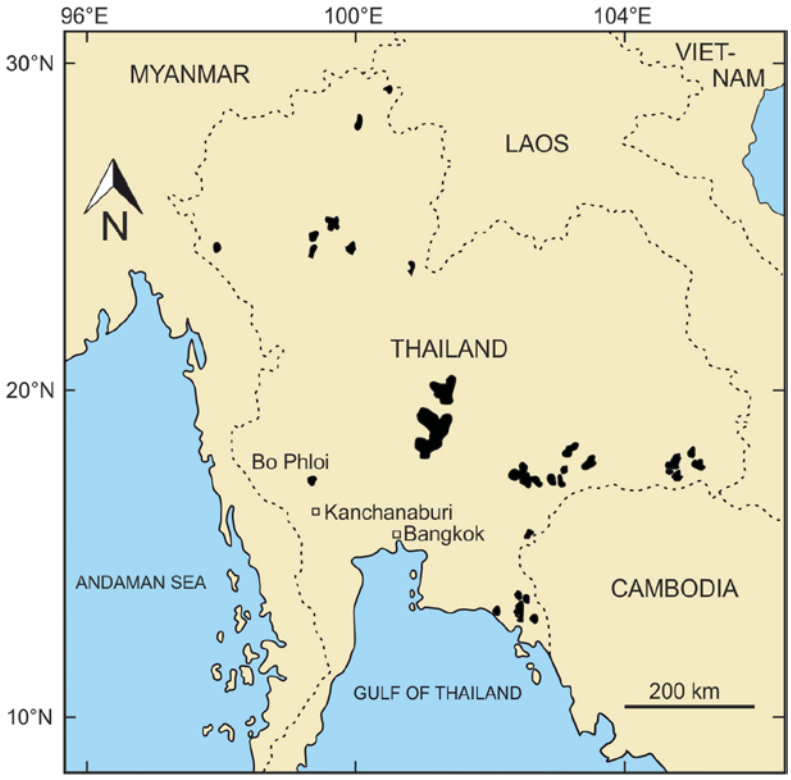

Figure 2: Simplified map showing the distribution of late Cenozoic basalt bodies (black patches) in Thailand, including the Bo Phloi occurrence. Modified after Limtrakun (2003).

Figure 3: **(a)** Image of a fingernail-sized spinel grain embedded in its host rock. **(b)** Areal view of the Bo Phloi mining site (March, 2012). Photos by B. Wanthanachaisaeng.

2. MATERIAL AND METHODS

The material investigated in the present study was collected in Bo Phloi and purchased from local dealers in September, 2018. It included several rough, more or less idiomorphic specimens of octahedral shape (Figure 1a; weights 4.8–6.75 g corresponding to 24.0–33.7 ct) and a few cut (faceted or carved) and polished specimens (Figs. 1a,b).

Rough spinel specimens were cut in half (at random orientation) using a Struers AWS1 abrasive wire saw, with a 0.17 mm diameter high-grade steel wire coated with 20 μm diamond grains (Well Diamantdrahtsägen GmbH, Mannheim). One half each was then embedded in epoxy, and ground and polished. For electron-beam imaging and major-element analysis, the sample mounts were coated with carbon. For optical absorption spectroscopy, thin doubly-polished slabs were prepared. For Mössbauer and X-ray powder diffraction analysis, sample material was powdered with an agate mortar and pestle.

To determine the mass density, five spinel specimens were weighed in air and in distilled water (a drop of liquid soap was added to reduce surface tension thus inhibiting the formation of bubbles). The refraction was measured with a Krüss ER601 refractometer. All measurements were repeated two times.

An X-ray powder diffraction analysis was performed with a Bruker D8 ECO powder diffractometer coupled with a LynxEye XET energy-dispersive detector. As radiation source Cu-K_α was used. The system was operated at 40 kV and 25 mA. The scanning range was between 5–140° 2Θ with 0.01° Θ step width. The analysis was performed with a fixed divergence slit and sample spinning setup. For X-ray powder diffraction data refinement, the software TOPAS version 4.2 (Bruker-AXS, 2009) was used.

Major element analyses were carried out by means of a CAMECA SX100 electron probe micro-analyser (EPMA). The instrument was operated in wavelength-dispersive mode with the following conditions: accelerating voltage 15 kV, current 20 nA, and diameter of the electron beam at the sample surface 2 μm. The following calibrant materials were used (the respective X-ray lines analysed are quoted in brackets): $MgAl_2O_4$ (Al–Kα, Mg–Kα), sanidine (Si–Kα), titanite (Ti–Kα), chromite (Cr–Kα), wollastonite (Ca–Kα), hematite (Fe–Kα), spessartine (Mn–Kα), vanadinite (V–Kα), gahnite (Zn–Kα), and Ni_2SiO_4 (Ni–Kα). Peak counting times were 10 s for major and 30 s for minor elements; the background counting times were half of the respective peak counting times. A X-PHI matrix correction routine (Merlet, 1994) was applied to the raw data. The Fe^{2+}/Fe^{3+} ratio was calculated from stoichiometry. Prior to EPMA analysis, back-scattered electron images (BSE) were acquired to check for possible zoning and other heterogeneity within the crystals.

Laser ablation–inductively coupled plasma–mass spectroscopy (LA–ICP–MS) measurements were carried out with an Agilent 7500cx quadrupole ICP–MS unit coupled with an ESI NWR–193 laser ablation system. The instrument was operated with a 193 nm laser, working at 8 Hz repetition rate pulse frequency with an energy of approximately 8 mJ/cm^2 at the surface and 75 μm spot size. A He gas flow set at 0.75 l/min transported the ablated material to the spectrometer unit. After every seventh measurement, NIST standard materials SRM610 and SRM612 glass

(Jochum et al., 2011) were probed for drift correction. The USGS reference glass BCR–2G (Rocholl, 1998) was measured for quality control and was reproduced within 10% relative error. Aluminium was used as an internal standard. The detection limits of this method are in the range 0.01–0.1 ppm for most trace elements. For data reduction, the software GLITTER 4.0 (Griffin et al., 2008) was utilized. Data for all elements were reduced using the SRM612 standard, except for ^{49}Ti for which the SRM610 standard was used.

Mössbauer analysis was performed with an apparatus manufactured by Halder Electronics GmbH. Measurement details are described elsewhere (Redhammer et al., 2012). Folded spectra were analysed applying the Voigt-based quadrupole-splitting distribution-approach (Rancourt and Ping, 1991; Lagarec and Rancourt, 1997). In here, distributions of quadrupole splitting due to slightly different local distortion environments around the Fe-probe site can be adequately modelled.

An optical absorption spectrum was measured in the near ultraviolet, visible, and near infrared spectral ranges. The instrument used was a Bruker IFS 66v/S Fourier-transform spectrometer. Analytical details are analogous to that of Zeug et al. (2018).

Raman spectroscopic measurements were performed with a Horiba LabRAM HR Evolution spectrometer. Measurement setups were the same as in Zeug et al. (2012). Spectra were excited with the 532 nm emission of a Nd:YAG laser (10 mW at the sample surface). Even though the resulting energy density was well below the threshold of any sample changes, as could possibly be caused by local heavy light absorption, all Raman analyses were carried out prior to EPMA and LA–ICP–MS analysis to avoid any possible bias.

3. RESULTS AND DISCUSSION

3.a Generalities

All samples are non-transparent and macroscopically black. Rough crystals appear matt and greyish black whereas polished specimens (faceted stones and carvings) have deep black colour and high lustre (Figure 1). The material's Mohs hardness is 8. This, along with the chemical stability and the lack of clear cleavage, explains samples' resistance to chemical and mechanical weathering. Note that, because of its hardness, the material has no streak colour.

The X-ray diffraction pattern of the Bo Phloi material corresponds to that of Mg-Al spinel. The unit-cell constant was determined at a_0 = 8.1363(1) Å, which corresponds well to literature data (a_0 = 8.103 Å; Putnis, 1992). The resulting cell volume is V=538.62(2) Å^3.

Samples were found to be optically isotropic, without any pleochroism. The refractive index was determined at 1.77, which is somewhat higher than the refraction of Mg-Al spinel (1.72; Koch and Sztrókay, 1966). The mean mass density was determined at 3.85 ± 0.1 g/cm^3, which is notably higher compared to that of Mg-Al spinel (3.64 g/cm^3; Koch and Sztrókay, 1966) but corresponds very well to a mass

density of 3.86 g/cm^3 determined by Saminpanya et al. (2008) for black spinel from Bo Phloi. This, along with the intense colour, points to an elevated presence of non-formula elements (for instance discussed in Koch and Sztrókay, 1966). The specimens did not show any magnetic properties.

3.b Chemical composition

The chemical composition of the black spinel from Bo Phloi has been determined by EPMA and LA–ICP–MS analysis; results are presented in Table I. Samples generally contain 59 wt% Al_2O_3, 19 wt% MgO, and 21wt% FeO (with the total Fe expressed as FeO). The measured values agree with the results of a previous study on black spinel from Bo Phloi (Saminpanya et al., 2008). In general, the Bo Phloi material contains low amounts of non-formula elements (below 0.2 wt%), with the exception of Fe and Ti. The BSE images of samples are virtually without any internal contrast. This, and generally low variations of EPMA results within and among samples, indicate that the Bo Phloi spinel has a fairly homogeneous chemical composition.

In spite of the significant Fe(total) content, the material is assigned to spinel *sensus stricto* (that is, Mg-Al spinel; Figure 4). The EPMA results were converted to end-member fractions, which resulted in a nominal composition of 72 mol% spinel (Mg-Al), 18 mol% hercynite (Fe^{2+}–Al^{3+}), 8.1 mol% magnetite (Fe^{2+}–Fe^{3+}), and 1.3 mol% ulvöspinel (Ti^{3+}–Fe^{2+}) components. Correspondingly, the data plot near the spinel end-member of the (Mg-Al)spinel–hercynite–magnetite triangle (Figure 4).

Table I. Mean chemical composition of black spinel from Bo Phloi.

EPMA results (n = 34)		LA–ICP–MS results (n = 14)					
Oxide	Concentration (wt%)*	Element	Isotope measured	Concentration (ppm)*	Element	Isotope measured	Concentration (ppm)*
SiO_2	0.16 ± 0.02	Li	7	0.74 ± 0.14	Ga	71	209 ± 3
TiO_2	0.66 ± 0.05	Be	9	0.14 ± 0.04	Sr	88	0.02 ± 0.01
Al_2O_3	59.0 ± 0.6	P	31	20.6 ± 3.4	Y	89	0.01 ± 0.01
MgO	18.7 ± 0.3	Ti	49	3440 ± 34	Zr	90	0.80 ± 0.18
FeO	20.7 ± 0.9	V	51	705 ± 7	Nb	93	0.03 ± 0.01
Cr_2O_3	0.05 ± 0.05	Cr	53	253 ± 5	Sn	118	0.29 ± 0.05
MnO	0.13 ± 0.02	Mn	55	1025 ± 9			
V_2O_3	0.12 ± 0.02	Co	59	283 ± 3			
ZnO	0.11 ± 0.02	Ni	60	1290 ± 19			
NiO	0.15 ± 0.03	Cu	63	2.94 ± 0.38			
Total	99.8 ± 0.3	Zn	66	1290 ± 23			

* All errors are quoted at the 1σ level.

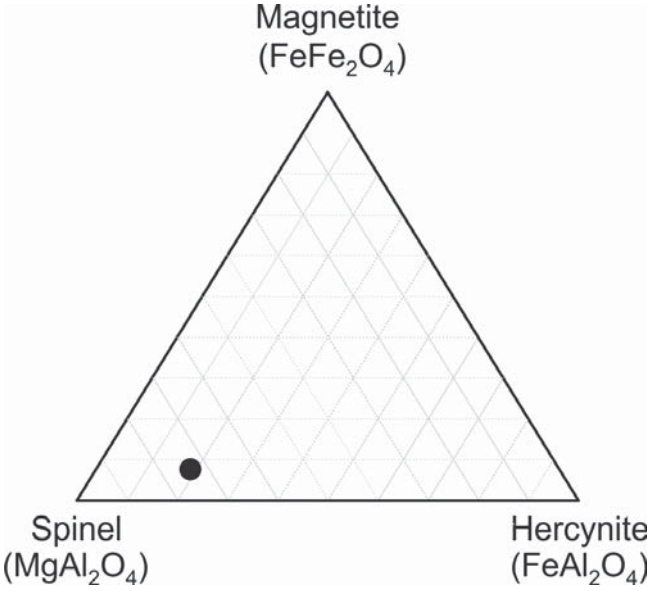

Figure 4: Results of chemical analyses (converted to nominal end-member fractions in mol%) plotted in the spinel end-member triangle. Note that 0.8 mol% ulvospinel ($TiFe_2O_4$) component exists but cannot be shown in this plot.

3.c Mössbauer spectroscopy

Mössbauer spectra (Figure 5) are characterized by a broad resonance absorption which can be resolved in three principal sites, based on their isomer shift and quadrupole splitting values. Two of these sites belong to Fe^{3+} and the third to Fe^{2+}. As it is typically found in Al-rich spinel samples, the Fe^{2+} contribution is broad and consists of three sub-components. This is in accordance with literature data (Larsson et al., 1994; Carbonin et al., 1996; Carbonin et al., 1999; Jastrzebska et al., 2017).

Refinement of the Mössbauer spectra showed that the broad component (being the sum of three sub-components) at the isomer shift of ~ 0.95 mm/s (Figure 5) is characteristic for Fe^{2+} in 4-coordination. The component with an isomer shift of ~ 0.35 mm/s is ascribed to Fe^{3+} in 6-coordination. The remaining component has isomer shifts and quadrupole splitting values typical of Fe^{3+} in 4-coordination. Note that fits were also done without assuming the presence of this last component ($Fe^{3+[4]}$). As the results were distinctly worse for these fits, it may be assumed that indeed there is a small amount of $Fe^{3+[4]}$ present. The fit results are presented in Table II. Note that Mössbauer spectra do not yield an independent indication for the presence of Fe^{2+} in octahedral position.

Under due consideration of the Mössbauer results, the chemical formula calculated from EPMA results (Table I) is estimated, based on four oxygen atoms per formula unit, as $(Mg_{0.66}Fe^{2+}_{0.30}Fe^{3+}_{0.04})^{[4]}_{\sum=0.99}$ $(Al_{1.80}Fe^{3+}_{0.11}Mg_{0.06}Ti_{0.01})^{[6]}_{\sum=1.98}$ O_4. Here, a small fraction of the Mg is assumed to be incorporated at the 6-coordiated site, as otherwise there would be a significant imbalance in the site occupations. The small but significant amounts of $Fe^{3+[4]}$ and $Mg^{2+[6]}$ characterise the cation occupation as “partially inverse”.

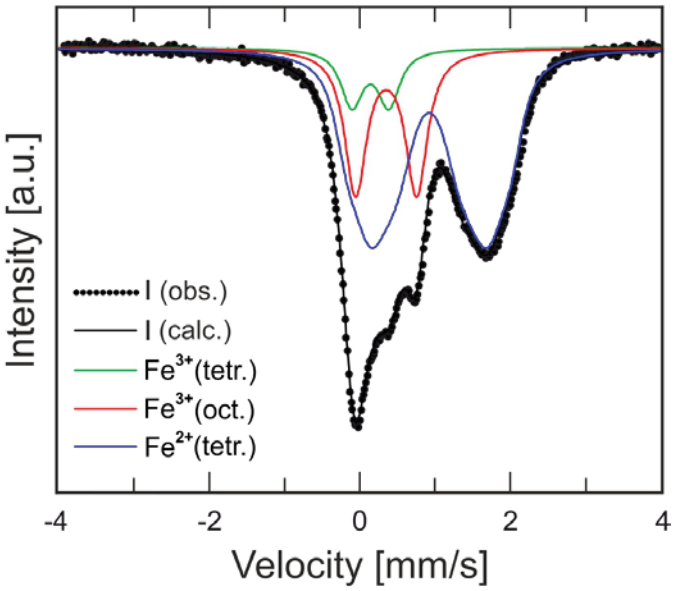

Figure 5: The Mössbauer spectrum of the Bo Phloi spinel indicates that there are three different iron species: Fe^{2+} in 4-coordination, and Fe^{3+} in 4- and 6-coordination.

Table II. Mössbauer parameters for the Bo Phloi spinel.

Iron species	Isomer shift (mm/s)	Quadrupole splitting (mm/s)	Area* (%)
Fe^{3+}; 4-coordinated	0.13 ± 0.2	0.5 ± 0.3	9 ± 1
Fe^{3+}; 6-coordinated	0.35 ± 0.2	0.8 ± 0.1	24 ± 1.5
Fe^{2+}; 4-coordinated	0.92 ± 0.2	0.9 ± 0.1 1.6 ± 0.1 2.2 ± 0.1	67 ± 1

*Area = integrated area of the respective doublet(s), normalised to 100%.

3.d Optical absorption spectroscopy

The optical absorption spectrum is shown in Figure 6. To quantify specific band positions, a twofold procedure was applied. First, several versions of “rubber-band corrections” based on polynomials with manually selected anchor points were performed, to account for the assumed shape of the absorption edge and for linear background absorption. Second, band deconvolution implying six Gaussian band profiles was performed. The final band positions were obtained by averaging the band fitting results of several background-subtracted spectra. It was found that the band positions do not vary too much, depending on which background correction was applied; whereas the bandwidths were quite different in some cases. The final band positions and a summary of their assignments are presented in Table III. The final spectrum is shown in Figure 6 as linear absorption coefficient plotted against wavenumber (lower abscissa axis) and wavelength (top abscissa axis).

Note, however, that even a 27 µm thick slab (see inset transmitted-light image in Figure 6) turned out to be too thick for obtaining an optical absorption spectrum

with adequate signal-to-noise ratio. The final spectrum presented in Figure 6 was, therefore, obtained from a thinned edge of the slab (10 μm thickness). As the material's chemical composition is very homogeneous, the small sample volume that was effectively analysed in the absorption spectrometer is not believed to cause any bias.

The comparatively sharp lowest energy band at 5280 cm^{-1} (full width at half maximum ~1700 cm^{-1}) is the result of the spin-allowed d–d crystal field transition of Fe^{2+} in the tetrahedral coordination, i.e. $^5E(D) \rightarrow {}^5T_2(D)$. Since this crystal field transition is affected by dynamic Jahn–Teller splitting, the observed band represents the high-energy component of the $^5T_2$ set only. Skogby and Hålenius (2003) identified three weaker split components at lower energies in infrared absorption spectra; the major one located at 3430 cm^{-1}. The assignment of the broad band at 10470 cm^{-1} is less clear than that of the lowest energy band. In this case, no major crystal field transition is to be expected due to the rather evidently low content of octahedral Fe^{2+}, not detected in the Mössbauer spectra. However, even limited contents of $Fe^{2+[6]}$ possibly cause the transition of exchange-coupled six-coordinated Fe^{2+}–Fe^{3+} pairs (ECP) at octahedral sites in the spinel structure, in accordance with the assignment of a comparable band by Hålenius et al. (2002). The quite flat and broad band at 14770 cm^{-1} is assigned, again in agreement with Hålenius et al. (2002), to electronic intervalence charge transfer (IVCT) between neighbouring six-coordinated Fe^{2+}–Fe^{3+} ions. This explanation is in contrast with the Mössbauer results too, as it also assumes some Fe^{2+} ions in the octahedral site. Worth mentioning is that even the slightest amounts of Fe^{2+} in the octahedron can be enough to activate the IVCT process.

Bands at higher energies have a high probability of relation to spin-forbidden d–d transitions of tetrahedral Fe^{2+} and/or octahedral Fe^{3+}. The apparently weak band at 17940 cm^{-1} may be attributed to the more or less field-independent spin-forbidden $^3E(G)$ level of $Fe^{2+[4]}$, perhaps with contributions from $^3T_1(H)$, $^3T_2(H)$ and/or $^3T_1(G)$. The well-articulated band at 21140 cm^{-1} typically results from spin-forbidden d–d transitions in six-coordinated Fe^{3+}, i.e. $^6A_1(S) \rightarrow {}^4A_1/{}^4E(G)$, probably mixed with spin-forbidden d–d transition in the tetrahedral Fe^{2+} position, e.g. $^5E(D) \rightarrow {}^3T_2(G)$. The shoulder centred at ~ 25400 cm^{-1} within the ligand–metal charge transfer (LMCT) absorption edge is also assumed to be related to a combination of spin-forbidden d–d transition of tetrahedral Fe^{2+} and octahedral Fe^{3+} positions, tentatively $^5E(D) \rightarrow {}^3T_2(D)$/ $^3T_2(P2)$ of $Fe^{2+[4]}$ and $^6A_1(S) \rightarrow {}^4T_2(D)$ of $Fe^{3+[6]}$.

In summary, the interpretation of the bands at 5280 cm^{-1}, 10470 cm^{-1} and 14770 cm^{-1} go along with the findings of Hålenius et al. (2002) who analysed samples with roughly comparable composition to this study's material. However, it needs to be noted that due to distinct differences in the composition and Fe distribution of the two materials (especially concerning a significantly higher octahedral Fe^{3+} content in our sample), explanation of the bands at 10470 cm^{-1} and 14770 cm^{-1} may not appear straightforward and unambiguous.

According to Taran et al. (2005), an absorption band around 10500 cm^{-1} can be assigned to electronic spin-forbidden transitions $^6A_{1g} \rightarrow {}^4T_{1g}$ of six-coordinated Fe^{3+}. Bands at 25410 cm^{-1}, 21140 cm^{-1}, and 17940 cm^{-1} correlate well with the measured band positions and interpretations of Andreozzi et al. (2001).

Table III. Assignment of optical absorption bands to their causal crystal-field phenomena.

Band position (cm^{-1})	Band position (nm)	Assignment
5280	1894	Spin-allowed d–d transition in $Fe^{2+[4]}$; $^5E(D) \rightarrow {}^5T_2(D)$
10470	955	Transition in exchange-coupled $Fe^{2+[6]} – Fe^{3+[6]}$ pairs (ECP) at octahedral sites
14770	677	Electronic charge transfer between neighbouring $Fe^{2+[6]} – Fe^{3+[6]}$ ions
17940	557	Spin-forbidden d–d transition in $Fe^{2+[4]}$; $^5E(D) \rightarrow {}^3T_2(H)$ [assignment uncertain]
21140	473	Spin-forbidden d–d transition in $Fe^{3+[6]}$; $^6A_{1g} \rightarrow {}^4A_{1g}$ and/or spin-forbidden d–d transition in $Fe^{2+[4]}$; $^5E(D) \rightarrow {}^3T_2$ [assignment uncertain]
25410	394	Spin-forbidden d–d transition in $Fe^{2+[4]}$; $^5E(D) \rightarrow {}^3E, {}^3T_2, {}^3T_1$ [assignment uncertain]

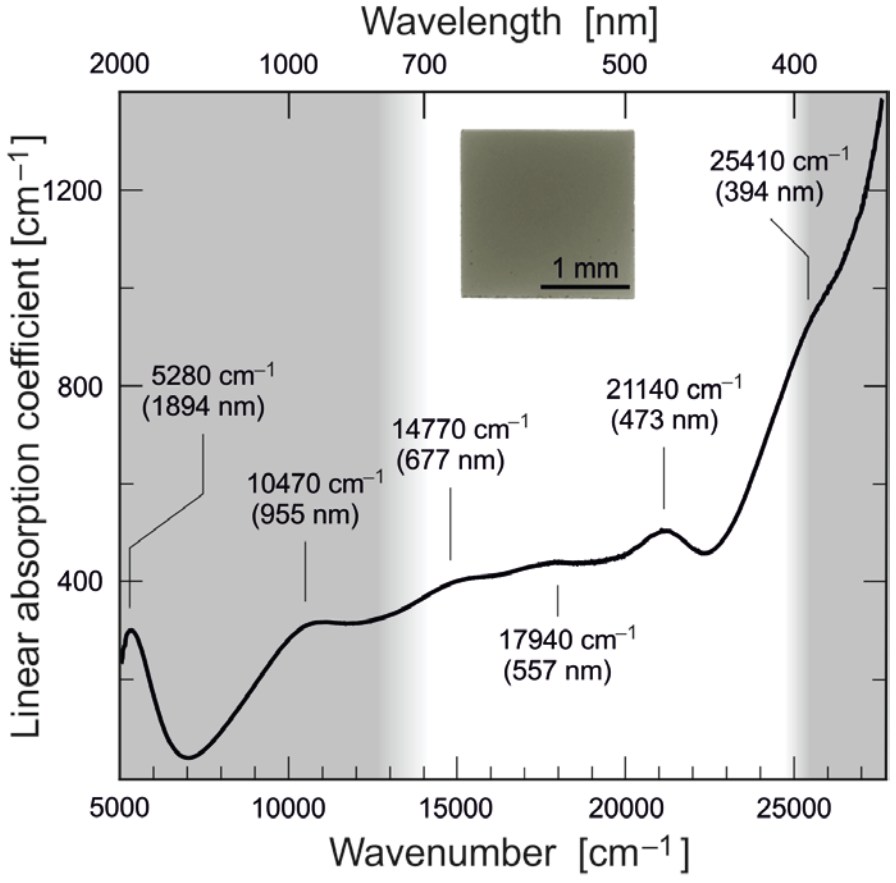

Figure 6: Optical absorption spectrum of spinel from Bo Phloi, measured in transmission mode from a 10 µm thick slab. Spectral ranges that are invisible to the human eye are indicated by grey background shade. The inset shows the 27 µm thick slab (transmitted-light photomicrograph); note the greyish brown colour.

3.e Raman spectroscopy

Raman spectrum of the black spinel from Bo Phloi (red spectrum) is shown in Figure 7, along with reference spectra of spinel *sensus stricto* (Nasdala et al., 2001), magnesiferrite, hercynite (D'Ippolito et al., 2015), and magnetite (Stähle et at., 2017). The spectrum is dominated by intense bands at 544 cm^{-1} and 749 cm^{-1}; which concurs with a Raman spectrum obtained from Bo Phloi spinel material by Saminpanya et al. (2008).

It is most striking that the Raman spectrum of the Bo Phloi spinel does not resemble the spectrum of "normal" Mg-Al spinel (Nasdala et al., 2001), that is, its most intense Raman bands at observed at different spectral positions and with different relative intensities (Figure 7). In contrast, the Raman spectrum of the Bo Phloi spinel shows similarities to that of the "inverse" spinel-group minerals hercynite and magnesioferrite (Figure 7). Andreozzi et al. (2001), D'Ippolito (2015) and Lenaz and Lughi (2017) have discussed that the Raman spectra of spinel-group minerals are controlled predominantly by the degree of "inversion" in the occupation of the two non-equivalent cation sites, rather than by the chemical composition alone. Lenaz and Lughi (2017) found that at low inversion degrees ($i \leq 0.14$), spinel spectra are still dominated by the strong 400–410 cm^{-1} Raman band of "normal" spinel (cf. Figure 7). The low intensity or even absence of this band in the Raman spectrum of the Bo Phloi spinel suggests that its degree of "partial inversion" must be significant; higher compared to the estimated chemical formula ($i \sim 0.04–0.06$).

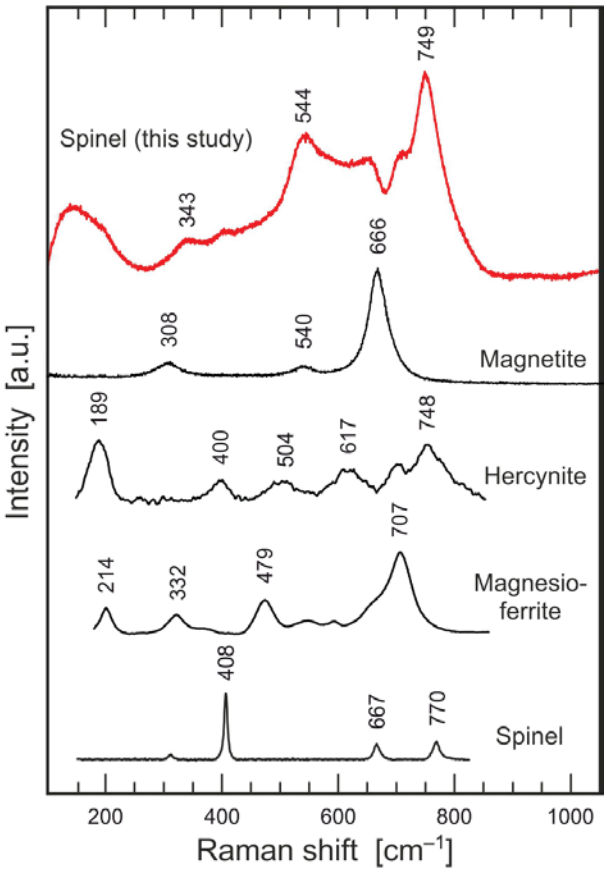

Figure 7: Raman spectrum of the Bo Phloi spinel in comparison with reference spectra. The dissimilarity of the spectrum of the Bo Phloi sample to that of (Mg-Al) spinel, and its similarity to the magnesioferrite spectrum, are explained by the "partially inverse" cation occupation. The reference spectrum of magnetite was obtained from a sample from Rumpersdorf, Austria (courtesy Eugen Libowitzky). The other reference spectra were extracted from D'Ippolito et al. (2015; magnesioferrite, hercynite) and Nasdala et al. (2001; spinel).

4. CONCLUSIONS

Black spinel from Bo Phloi, Thailand, is characterised by a remarkably homogenous chemical composition, corresponding to $MgAl_2O_4$ with particularly high Fe content. Mössbauer spectroscopic results indicate that $Fe^{2+[4]}$ represents 67%, $Fe^{3+[6]}$ 24%, and $Fe^{3+[4]}$ 9% of the total Fe (Table II). The presence of $Fe^{2+[6]}$ is indicated by the optical absorption spectrum; however, the content of this Fe species was found to be below the detection limit of Mössbauer spectroscopy. The chemical formula (based on 4 O per formula unit), estimated from EPMA and Mössbauer spectroscopic data, is $(Mg_{0.66}Fe^{2+}_{0.30}Fe^{3+}_{0.04})^{[4]}_{\sum=0.99}$ $(Al_{1.80}Fe^{3+}_{0.11}Mg_{0.06}Ti_{0.01})^{[6]}_{\sum=1.98}$ O_4, representing a "partially inverse" occupation of the two cation sites. Concurring with the above, the Raman spectrum also indicates that the Bo Phloi spinel does not represent a "normal" but rather a "partially inverse" cation occupation. A strong absorption edge detected by optical absorption spectroscopy causes the non-transparent, intensive dark coloration of the mineral. Bands in the visible range are responsible for greyish brown colours that can only be observed in a <0.1 mm thin slab.

5. REFERENCES

Andreozzi G.B., Hålenius U. and Skogby H., 2001. Spectroscopic active $^{IV}Fe^{3+}$–$^{VI}Fe^{3+}$ cluster in spinel-magnesioferrite solid solution crystals: a potential monitor for ordering in oxide spinels. *Physics and Chemistry of Minerals*, **28**, 435–444, https://dx.doi.org/10.1007/s002690100178.

Barr S.M. and Macdonald A.S., 1981. Geochemistry and geochronology of Late Cenozoic basalts of Southeast Asia – part II. *Geological Society of American Bulletin*, **92**, 1069–1142, https://dx.doi.org/10.1130/GSAB-P2-92-1069.

Barr S.M. and Macdonald A.S., 1978. Geochemistry and petrogenesis of late Cenozoic alkaline basalts of Thailand, *Geological Society of Malaysia Bulletin,* **10,** 25–52.

Bruker-AXS (2009) *TOPAS version 4.2 - software for powder diffraction data*. Karlsruhe, Germany

Bunopas S. and Bunjitradulya S., 1975. Geology of Amphoe Bo Ploi, North Kanchanaburi with special notes on the "Kanchanaburi Series". *Journal of the Geological Society of Thailand,* **1**, 51–67.

Carbonin S., Menegazzo G., Lenaz D. and Princivalle F., 1999. Crystal chemistry of two detrital Cr-spinels with unusually low values of oxygen positional parameter: oxidation mechanism and possible origin. *Neues Jahrbuch Für Mineralogie–Monatshefte,* **8**(8), 359–371.

Carbonin S., Russo U. and Della Giusta A., 1996. Cation distribution in some natural spinels from X-ray diffraction and Mössbauer spectroscopy. *Mineralogical Magazine,* **60**(399), 355–368, https://dx.doi.org/10.1180/minmag.1996.060.399.10.

Choowong M., 2002. Quaternary geology and sapphire deposits from the Bo Phloi gem field, Kanchanaburi Province, Western Thailand. *Journal of Asian Earth Sciences*, **20**(2), 119–125, https://dx.doi.org/10.1016/S1367-9120(01)00032-3.

Deer W.A., Howie R.A. and Zussman J., 1996. *An introduction to the rock-forming minerals*, 2nd edn. Longman Scientific and Technical, Harlow, 696 pp.

D'Ippolito V., 2013. *Linking crystal chemistry and physical properties of natural and synthetic spinels: an UV-VIS-NIR and Raman study*. Ph.D thesis, Sapienza Università di Roma, Rome.

D'Ippolito V., Andreozzi G.B., Bersani D. and Lottici P.P., 2015. Raman fingerprint of chromate, aluminate and ferrite spinels. *Journal of Raman Spectroscopy*, **46**(12), 1255–1264, https://dx.doi.org/10.1002/jrs.4764.

Griffin W.L., Powell W.J., Pearson N.J. and O'Reilly S.Y., 2008. Glitter: Data reduction software for laser ablation ICP–MS. In Sylvester P.J., Ed., *Laser ablation ICP–MS in the Earth sciences: Current practices and outstanding issues*. Mineralogical Association of Canada (Vancouver, BC, Canada) Short Course, **40**, 308–311.

Grimes N.M., Thompson P. and Kay H.F., 1982. New symmetry and structure for spinel. *Proceedings of the Royal Society of London*, **386**, 333–345.

Hålenius U., Skogby H. and Andreozzi, G.B., 2002. Influence of cation distribution on the optical absorption spectra of Fe^{3+}-bearing spinel s.s.– hercynite crystals: evidence for electron transitions in $^{VI}Fe^{2+}$–$^{VI}Fe^{3+}$ clusters. *Physics and Chemistry of Minerals*, **29**, 319–330, https://dx.doi.org/10.1007/s00269-002-0240-z.

Hansawek R. and Pattamalai K., 1997. Kanchanaburi sapphire deposits. *Mineral Resources Gazette*, **45**(1), 17–38.

Hawthorne F.C., 1988. Mössbauer Spectroscopy. In F.C. Hawthorne, Ed., *Spectroscopic Methods in Mineralogy and Geology*, De Gruyter, Boston, 255–340.

Hurwit K.N., 1988. Gem trade lab notes: Augite, Chinese "onyx". *Gems and Gemology,* **24**(3), 170.

Jastrzebska I., Bodnar W., Witte K., Burkel E., Stoch P. and Szczerba J., 2017. Structural properties of Mn-substituted hercynite. *Nukleonika,* **62**(2), 95–100, https://dx.doi.org/10.1515/nuka-2017-0013.

Jochum K.P., Weis U., Stoll B., Kuzmin D., Yang Q., Raczek I., Jacob D.E., Stracke A., Birbaum K., Frick D.A., Günther D. and Enzweiler J., 2011. Determination of reference values for NIST SRM 610–617 glasses following ISO guidelines. *Geostandards and Geoanalytical Research*, **35**(4), 397–429, https://dx.doi.org/10.1111/j.1751-908X.2011.00120.x.

Khamloet P., Pisutha-Arnond V. and Sutthirat C., 2014. Mineral inclusions in sapphire from the basalt-related deposit in Bo Phloi, Kanchanaburi, Western Thailand: indication of their genesis*. Russian Geology and Geophysics,* **55**(9), 1087–1102, https://dx.doi.org/10.1016/j.rgg.2014.08.004.

Koch S. and Sztrókay K. I., 1966. *Mineralogy I.-II.* 2nd edn. Nemzeti Tankönyvkiadó, Budapest, 405 & 526 pp (in Hungarian).

Lagarec K. and Rancourt D.G., 1997. Beam interactions with materials and atoms. *Nuclear Instruments and Methods in Physics Research Section B*, **129**(2), 143–303.

Larsson L., Oneill H.S. and Annersten H., 1994. Crystal-chemistry of synthetic hercynite ($FeAl_2O_4$) from XRD structural refinements and Mossbauer-spectroscopy. *European Journal of Mineralogy,* **6**, 39–51.

Lenaz D. and Lughi V., 2017. Raman spectroscopy and the inversion degree of natural Cr-bearing spinels. *American Mineralogist*, **102,** 327–332.

Limtrakun P., 2003. *Origin and distribution of corundum from an intraplate alkali basaltic province in Thailand: evidence from field and inclusion studies*. Ph.D thesis, University of Tasmania, Hobart.

Merlet C., 1994. An accurate computer correction program for quantitative electron probe microanalysis. *Microchimica Acta*, **114/115**, 363–376.

Mukasa S.B., Fischer G.M. and Barr S.M., 1996. The character of the subcontinental mantle in Southeast Asia: evidence from isotopic and elemental compositions of extension-related Cenozoic basalts in Thailand. In A. Basu, S. Hart, Eds., Earth Processes: Reading the Isotopic Code, *Geophysical Monograph Series*, **95**, American Geophysical Union, Washington, D.C., 223–252.

Nasdala L., Banerjee A., Häger T. and Hofmeister W., 2001: Laser-Raman micro-spectroscopy in mineralogical research. *Microscopy and Analysis, European Edition*, **70**, 7–9.

Ngarmpis Y., 1982. *The petrochemical study of corundum-bearing basalts at Bo Phloi District, Kanchanaburi*. M.Sc. thesis, Chulalongkorn University, Bangkok.

O'Neill H.ST.C. and Navrotsky A., 1983. Simple spinels: crystallographic parameters, cation radii, lattice energies, and cation distribution. *American Mineralogist*, **68,** 181–194.

Putnis A., 1992. *Introduction to mineral sciences*. Cambridge University Press, https://dx.doi.org/10.1017/CBO9781139170383.

Rancourt D.G. and Ping J.Y., 1991. Voigt-based methods for arbitrary-shape static hyperfine parameter distributions in Mössbauer spectroscopy. *Nuclear Instruments and Methods in Physics Research Section B,* **58**(1), 85–97, https:// dx.doi.org/10.1016/0168-583X(91)95681-3.

Redhammer G.J., Tippelt G., Amthauer G. and Roth G., 2012. Structural and ^{57}Fe Mössbauer spectroscopic characterization of the synthetic $NaFeSi_2O_6$ (aegirine) – $CaMgSi_2O_6$ (diopside) solid solution series. *Zeitschrift für Kristallographie*, **227**, 396–410, https://dx.doi.org/10.1524/zkri.2012.1514.

Rocholl A., 1998. Major and trace element composition and homogeneity of microbeam reference material: basalt glass USGS BCR-2G. *Geostandards and Geoanalytical Research*, **22**(1), 33–45, https:// dx.doi.org/10.1111/j.1751-908X.1998.tb00543.x.

Saminpanya S. and Sutherland F.L., 2008. Black opaque gem minerals associated with corundum in the alluvial deposits of Thailand. *The Australian Gemmologist,* **23,** 242–253.

Sickafus K.E., Wills J.M. and Grimes N.W., 1999. Structure of Spinel. *Journal of the American Ceramic Society*, **82**(12), 3279–3292, https://dx.doi.org/10.1111/j.1151-2916.1999.tb02241.x.

Skogby H. and Hålenius U., 2003. An FTIR study of tetrahedrally coordinated ferrous iron in the spinel-hercynite solid solution. *American Mineralogist,* **88**(4), 489–492, https:// dx.doi.org/10.2138/am-2003-0402.

Sutthirat C., Charusiri P., Farrar E. and Clark A.H., 1994. New $^{40}Ar/^{39}$ Ar geochronology and characteristics of some Cenozoic basalts in Thailand. *Proceedings of International Symposium on Stratigraphic Correlation of Southeast Asia,* November 15–20, Bangkok, 306–321.

Stähle V., Altherr R., Nasdala L., Trieloff M. and Varychev A., 2017. Majoritic garnet grains within shock-induced melt veins in amphibolites from the Ries impact crater suggest ultrahigh crystallization pressures between 18 and 9 GPa. *Contributions to Mineralogy and Petrology*, **172**, 86.

Stauffer P., 1983. Unraveling the mosaic of paleozoic crustal blocks in Southeast Asia. *Geologische Rundschau,* **72**, 1061–1080.

Taran M.N., Koch-Müller M. and Langer K., 2005. Electronic absorption spectroscopy of natural (Fe^{2+}, Fe^{3+})-bearing spinels of spinel s.s.-hercynite and gahnite-hercynite solid solutions at different temperatures and high-pressures. *Physics and Chemistry of Minerals*, **32**, 175–188, https://dx.doi.org/10.1007/s00269-005-0461-z.

Udomchoke V., 1988. Quaternary stratigraphy of the Khorat Plateau area, Notheastern Thailand. In: N. Thiramongkol, Ed., *Proceeding of the workshop on correlation of Quaternary succession in South, East and Southeast Asia.* November 21–24, Bangkok, 69-95.

Vichit P., Vudhichativanich S. and Hansawek R., 1978. The distribution and some characteristics of corundum-bearing basalts in Thailand. *Journal of the Geological Society of Thailand,* **3**, M4–M38.

Yaemniyom N., 1982. *The petrochemical study of corundum-bearing basalts at Bo Ploi District, Kanchanaburi*. M.Sc. thesis, Chulalongkorn University, Bangkok.

Yu Y. and Gee J.S., 2005. Spinel in Martian meteorite SaU 008: implications for Martian magnetism. *Earth and Planetary Science Letters*, **232**(3–4), 287–294, https://dx.doi.org/10.1016/j.epsl.2004.12.015.

Xirouchakis D., Draper D.S., Schwandt C.S. and Lanzirotti A., 2002. Crystallization conditions of Los Angeles, a basaltic Martian meteorite. *Geochimica et Cosmochimica Acta*, **66**(10), 1867–1880, http:// dx.doi.org/10.1016/S0016-7037(01)00892-4.

Zeug M., Nasdala L., Wanthanachaisaeng B., Balmer W.A., Corfu F. and Wildner M., 2018. Blue Zircon from Ratanakiri, Cambodia. *The Journal of Gemmology*, **36**(2), 112–132, https://dx.doi.org/10.15506/JoG.2018.36.2.112.

6. LIST OF FIGURES

7. LIST OF TABLES

ERKLÄRUNG

Hiermit versichere ich, Ágnes Blanka Kruzslicz

- dass ich die vorliegende Masterarbeit selbständig verfasst, andere als die angegebenen Quelle und Hilfsmittel nicht benutzt und mich auch sonst keiner unerlaubter Hilfe bedient habe,
- dass ich dieses Masterarbeitsthema bisher weder im In- noch im Ausland in irgendeiner Form als Prüfungsarbeit vorgelegt habe, und
- dass diese Arbeit mir der vom Begutachter beurteilten Arbeit vollständig übereinstimmt.

Wien, am 29.07.2019